The Astronomical Journal, 163:102 (6pp), 2022 February https://doi.org/10.3847/1538-3881/ac32dd


# A Search for Planet Nine using the Zwicky Transient Facility Public Archive

Michael E. Brown and Konstantin Batygin
Division of Geological and Planetary Sciences California Institute of Technology, Pasadena, CA 91125, USA; mbrown@caltech.edu
*Received 2021 September 2; revised 2021 October 18; accepted 2021 October 22; published 2022 January 31*

## Abstract

Recent estimates of the characteristics of Planet Nine have suggested that it could be closer than originally assumed. Such a Planet Nine would also be brighter than originally assumed, suggesting the possibility that it has already been observed in wide-field moderate-depth surveys. We search for Planet Nine in the Zwicky Transient Facility public archive and find no candidates. Using known asteroids to calculate the magnitude limit of the survey, we find that we should have detected Planet Nine throughout most of the northern portion of its predicted orbit—including within the galactic plane—to a 95% detection efficiency of approximately $V = 20.5$. To aid in understanding detection limits for this and future analyses, we present a full-sky synthetic Planet Nine population drawn from a statistical sampling of predicted Planet Nine orbits. We use this reference population to estimate that this survey rules out 56% of predicted Planet Nine phase space, and we demonstrate how future analyses can use the same synthetic population to continue to constrain the amount of parameter space effectively searched for Planet Nine.

*Unified Astronomy Thesaurus concepts:* Sky surveys (1464); Transient sources (1851); Solar system planets (1260); Solar system astronomy (1529)

## 1. Introduction

The unexpected alignment of both the longitudes of perihelion and the orbital poles of distant detatched Kuiper Belt objects (KBOs) with semimajor axes beyond 150 au suggests the existence of a giant planet well beyond the Kuiper Belt (Batygin & Brown 2016). The preliminary estimates of the orbital parameters of this planet—which we will call Planet Nine here—suggested that the planet could have a semimajor of 700 au or greater and a visual magnitude of 24 or fainter. Several observational searches are currently underway for this hypothesized planet using large telescopes capable of reaching such faint distant objects.

Recently, (Brown & Batygin 2021; hereafter BB21) developed a method to use the full set of detections of distant detached KBOs, along with estimates of the biases in these detections and a large suite of numerical simulations, to make a statistical model for the orbital parameters of Planet Nine. The posterior distribution for the predicted distance to Planet Nine is broad, but one important outcome of the analysis is the realization that Planet Nine could possibly be both closer and less massive than originally assumed. Even though a less massive planet will likely be slightly smaller, the closer distance to the planet can make it as much as 2 magnitudes brighter than the original estimates. Planet Nine may not require dedicated searches on large telescopes but, instead, may have been already imaged in one of the increasingly large numbers of wide-field surveys completed or underway to date.

Here, we search the first 3 yr of the public Zwicky Transient Facility (ZTF) archives for Planet Nine using a new orbit-linking algorithm that is efficient at searching sparsely sampled data across multiple opposition. To understand the effectiveness of our search we develop a method to calibrate the efficiency of the ZTF observations using both detections and nondetections of known asteroids within the ZTF survey. The survey method and calibration are applicable to other large-scale transient surveys currently underway.



## 2. ZTF Data

Our orbit-linking method and calibration are agnostic to how and where the data are acquired. Instead, our self-calibration accounts for the characteristics of the survey depth and cadence with no preknowledge. Nonetheless, we briefly introduce the key characteristics of the ZTF public survey here. The ZTF is a time-domain survey run on the Samuel Oschin 48 Schmidt telescope at Palomar Observatory. The CCD camera covers a 47 deg$^2$ field of view. The public survey nominally covers the full sky visible north of $-30°$ decl. once every three nights. In addition, a strip approximately 10° wide centered on the galactic plane is imaged nightly. The 15 s exposures of the survey reach a $5\sigma$ reported depth of $g = 20.8$ and $r = 20.6$, though significant variations occur (Bellm et al. 2019). Astometric registration of the frame to GAIA is good to 30 ms, and the faintest sources cataloged have uncertainties of $\sim 1''$ (Masci et al. 2019). The archive begins with data on 2018 June 1 and continues to be updated nightly. We restrict our analysis to data from 2018 June 1 until 2021 May 7 and to the specific region on the sky predicted for the location of Planet Nine by BB21, The ZTF data cover essentially every location along the predicted path of Planet Nine many times over on many separate dates with the exception of the furthest southern portion of the orbit.

The ZTF public archive contains only nightly transients, that is, detections on the image made after a reference template has been subtracted (Masci et al. 2019). Such transients are ideal for detecting moving objects in the solar system. Every morning, we download the full set of nightly transients from the archive page.[1] Many real astrophysical transients will repeat sporadically or stay bright for multiple nights; we thus

[1] http://ztf.uw.edu/alerts/public

discard any transients that appear more than once at a single location. As of 2018 June 1, the Planet Nine search area of the ZTF archive contains ∼13 million detections that fit this criteria, including 8.6 million within 2″ of known solar system objects (discussed further below). Nearly every other single-night transient is a false positive of some sort, but unknown bright solar system objects will also appear—possibly many times—in this catalog. Our task is to discard the many false positives and link any real objects onto Keplerian orbits to identify their existence.

## 3. Detection Limits

Before searching for Planet Nine itself, we develop a method to determine detection limits in the ZTF data. Little information on coverage, filling-factor, sky conditions, or other parameters that would be required to compute real search limits is available in the nightly public archive. We instead develop a method using known asteroids to self-calibrate the survey.

Every ZTF image—particularly near the ecliptic—contains many detections of asteroids, each of which will appear in the single-epoch transient catalog that we create. Numbered asteroids have sufficiently well-known orbits that they should appear at nearly precisely their predicted position. These asteroids also have predicted magnitudes. Unfortunately, the predicted magnitudes are not as reliable as the predicted positions. The predicted magnitudes do not account for light curves, colors, or individual phase functions. To determine how much the true magnitudes differ from the predicted magnitudes we examine 100,000 labeled asteroids and find that, accounting for offsets between $g$ and $r$ and the predictions, which are in $V$, the predictions have a root-mean-square (RMS) deviation of 0.2 magnitudes with respect to the observations. No systematic offsets are seen.

We will thus use these asteroids as known transient point sources of known magnitude to calibrate the efficiency of the survey, with the caveat that the calibration is uncertain to a few tenths of a magnitude. The benefit of using these asteroids is that, owing to the large number of asteroids on each image taken, they account for the efficiency of all aspects of the survey, from observing conditions at the moment of the image, to which regions of the sky are surveyed each night, to detector geometry, to transient processing pipeline.

We use JPL Horizons[2] to predict position and magnitudes at 1 day intervals across the 3 yr of the survey of every numbered asteroid. We then interpolate to the time of each image and look for transients within 2″ of each predicted asteroid position. We find that most of the asteroid associations are labeled in the ZTF archive, but a small number are not. Given the astrometric precision of ZTF and the well-known orbits of numbered asteroids, most of the detections are within an arcsecond of their predicted position.

For each night in the 3 yr period, we track each numbered asteroid that appears in the transient catalog and also each that could have appeared, but does not. We divide the sky into ∼1.8 square degree equal-area regions using an NSIDE = 32 HEALPix grid,[3] and we grid each detection and nondetection into 0.25 magnitude bins for each night of the 3 yr. Note that we exclusively use the predicted magnitude for both detected and undetected objects. While ZTF observes in multiple wavelength bands, we make no attempt at correcting for color; this procedure is equivalent to implicitly assuming that Planet Nine has the same color as the average asteroid. Within the limits of this calibration, this assumption should be adequate. For each night and at each position in the sky, we are thus able to estimate the probability that a moving object of a particular predicted magnitude is detected any night of the 3 yr survey.

As an initial estimate of the Planet Nine search efficiency, we can ask the question: what is the probability that an object of a given magnitude would be detected $n$ or more times at a particular location? Here, $n$ is the number of detections that we require to successfully detect Planet Nine. Smaller values of $n$ will make it more likely that enough detections of Planet Nine will have occurred, while increasing the probability of false linkages. Higher values of $n$ will lower our detection efficiency but likewise lower the false-positive rate. In addition, higher values of $n$ require less processing time for our detection algorithm, described below. Below, we find that $n \sim 7$ provides an attractive trade-off between these competing factors. For this initial detection limit estimation, we thus define our magnitude limit as the brightness at which there is a 95% or greater probability that an object at that magnitude would have been detected seven or more times. To determine this magnitude limit, we simulate 1000 observations in each HEALPix at each point in the magnitude grid on each night of the survey and determine the faintest object that is detected seven or more times 95% of the time. Our survey limit map is shown in Figure 1.

Several interesting features of the limit map are clear. First, the northern galactic plane is well-covered. Even with the high density of stationary sources in the plane causing confusion with transients, the high cadence—particularly within 10° of the plane—means that real moving objects have multiple opportunities to be detected throughout the year and are eventually detected seven or more times as efficiently as outside of the galactic plane. The southern galactic plane is less well-covered, owing to the 33° latitude of Palomar observatory, but regions of good coverage exist. The survey limit estimate is best where large numbers of asteroids are predicted or observed. At higher ecliptic latitudes the method fails. In principle one could estimate an efficiency based on stellar density and coverage, though we do not attempt that here.

In order to understand how strongly the number of detections required affects detection limit, we calculate a limit map for 14 required detections. Throughout most of the survey region, the limits are worse by no more than 0.25 magnitudes. The extremely large number of images obtained across the whole northern sky by ZTF ensure that a sufficiently bright Planet Nine will be detected many times in the survey.

## 4. A Planet Nine Reference Population

For calibration of our search algorithm, described below, and for eventual understanding of its detection limits, it will be helpful to define a Planet Nine reference population and simulate its detection. Indeed, this reference population is a useful tool beyond this analysis, as it will allow any survey to help understand which parts of the Planet Nine parameter space it has ruled out and which others have already been ruled out.

The Markov chain Monte Carlo analysis of BB21 created a posterior sample of orbital parameters for 49100 realizations of Planet Nine. For these realizations, 95% of the population is within a swath of sky ±12° in decl. from an orbit with an

[2] http://ssd.jpl.nasa.gov
[3] https://healpix.jpl.nasa.gov/html/idl.htm

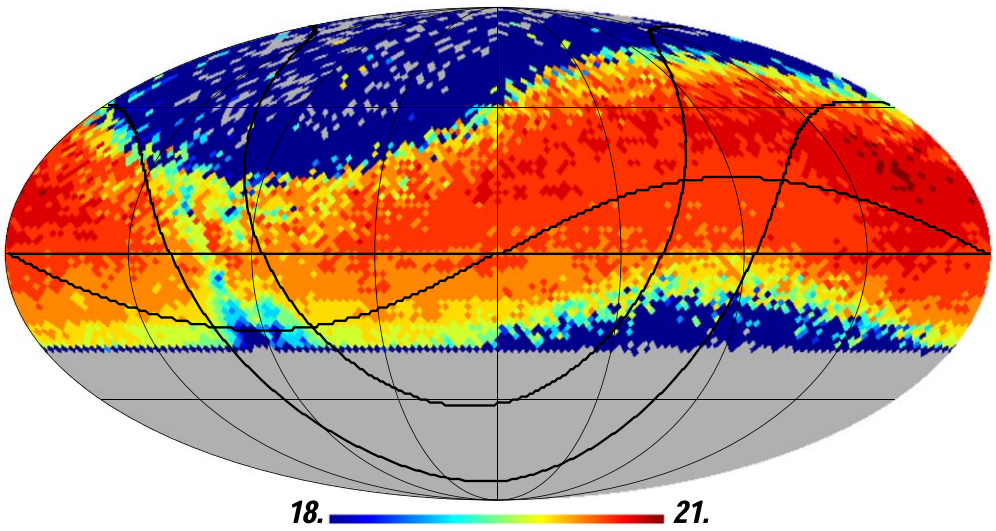


**Figure 1.** The $V$ magnitude at which there is a 95% or higher probability that a moving object would be detected seven or more times in the first 3 yr of the ZTF public survey. The Mollweide equal-area projection is centered at R.A. = 180° and decl. = 0° with R.A. increasing toward the left. The path of the ecliptic and ±15° of the galactic plane are highlighted. For much of the sky a uniform limit of $V \sim 20.5$ is attained, with slightly greater depth north of celestial equator. Despite the high density of stationary stars, the northern galactic plane has no worse depth than any other region of the sky. The higher density in the southern galactic plane and the lower declinations make this region the least well-covered. At high-ecliptic latitudes the small number of asteroids prevents accurate calculation of the limits.

inclination of 16° and an ascending node of 97°. The $1\sigma$ bounds on the population has a mass of $6.2^{+2.2}_{-1.3}$ Earth masses, a semimajor axis of $380^{+140}_{-80}$ au, and a perihelion distance of $300^{+85}_{-80}$ au.

We create our reference population of 100,000 potential Planets Nine by randomly selecting from the sample parameters 100,000 times and picking a random value of mean anomaly, $M$, between 0 and 360°. We use the same assumptions as BB21 for the radius and albedo, that is we assume a simple mass-diameter relationship of $r_9 = (m_9/3M_{\rm earth})\, R_{\rm earth}$ based on fits to planets in this radius and mass range by Wu & Lithwick (2013), and we assume a full range of albedos from 0.2—half that of Neptune—to 0.75, the value predicted by modeling from Fortney et al. (2016), who find that all absorbers are condensed out of the atmosphere and the planet should have a purely Rayleigh-scattering albedo.

This Planet Nine reference population contains a statistical sampling of orbital elements—including a mean anomaly at a defined epoch—and a mass, radius, and albedo for each member of our synthetic sample. The sample[4], can be used to predict the position and brightness of all members of the Planet Nine reference population for any future or past survey. We use this sample to predict position and magnitude for each night of the 3 year ZTF survey. We then use our asteroid-derived estimate of detection efficiency as a function of HEALPix, magnitude, and observing night, to determine the probability that each synthetic object would be observed on any given night. We select a uniform random number between 0 and 1 and, if the number is lower the probability of detect of an object of that magnitude, we record that object as detected at that position on that night.

As we will discuss below, we will require the detection of Planet Nine at least seven times over our 3 yr period. Based on the cadence of observations and our calculated magnitude limits, 56373 of the 100000 objects in the Planet Nine reference population would have been detected seven or more times in the ZTF survey. The undetected members of the reference are either too faint for the ZTF survey or south of the survey latitude limit. A total of 42,350 objects are detected as many as 25 times. These reference population detections show that, if we can develop an algorithm capable of linking seven or more Planet Nine-like orbits, the ZTF survey will be capable of ruling out more than 56% of potential Planet Nine parameter space.

## 5. Orbit Linking

Brown et al. (2015) developed a general method for linking single-epoch transient detections across multiple nights onto outer solar system orbits. The method involved calculating best-fit orbits to every possible set of three transient detections across a single opposition using the geocentric linear approximation of Bernstein & Khushalani (2000), which we refer to as the Bernstein method. For triplets with sufficiently small residuals in the linear approximation, full orbits were determined and residuals were determined. Only orbits with residuals below 1″ were retained. The large numbers of triplets were eventually combined to find low-residual quadruplet linkages and, for particularly contaminated regions, to quintuplets. For the data from the 8 yr of the Catalina Realtime Transient Survey, this process led to detections of all bright Kuiper Belt objects within the survey field with zero false positives, but zero new detections.

While effective, this method does not scale well to the larger surveys now becoming available. Recently, Holman et al. (2018) developed an alternative orbital approximation which greatly improves the ability to link multiple epochs even across multiple opposition. In the simplest version of the Holman method, objects are assumed to be moving at a constant speed in circular motion around the Sun. The observed position of an object is then transformed into heliocentric, rather than geocentric, coordinates, using a range of assumed distances and the known position of the Earth. In this coordinate system objects move on great circles in heliocentric coordinates at a constant speed when the correct distance is assumed, greatly

[4] Permanently archived at https://data.caltech.edu/records/2098 (Brown 2021).

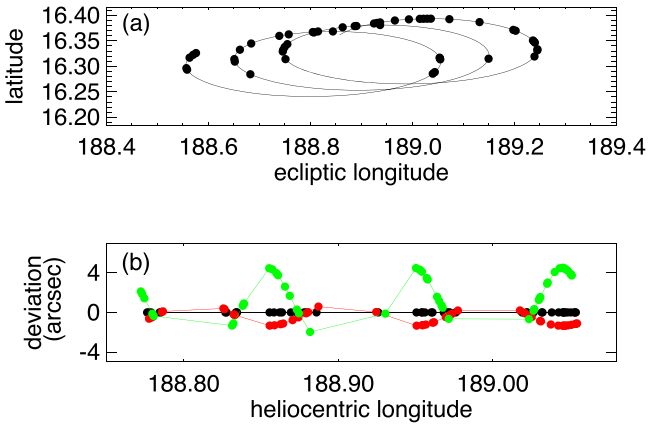


**Figure 2.** An example object from our Planet Nine reference population with a current distance of 264.8 au is predicted to have been detected 50 times in the ZTF survey. (a) Seen from the Earth, these detections make three loops over the three year survey period. (b) Transformed to heliocentric coordinates at the correct assumed distance (black), the object travels in a straight line at a constant speed. With an incorrect assumed distance of 263.2 au (red) or 270.3 au (green) deviations to the straight line motion can be seen.

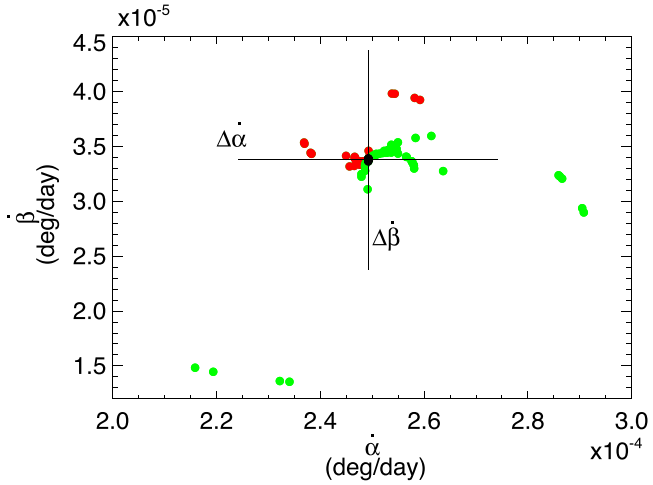


**Figure 3.** The speed in heliocentric longitude and in heliocentric latitude to travel from the first point in the orbit to each of the other 49 for our synthetic object shown in Figure 2. If the correct distance of 264.8 au is assumed, the speeds to all data points are nearly identical (black). With an incorrect assumed distance (263.2 au, red, and 270.3 au, green, as in Figure 2), the cluster of inferred speeds is larger. Our algorithm finds all clusters within the ranges of selected values of $\Delta\dot{\alpha}$ and $\Delta\dot{\beta}$ shown and would successfully identify all red (and black) detections as clustered. With the incorrect distance assumed for the green cluster, many of the points would not be identified.

simplifying linking (Figure 2). This method is increasingly efficient at larger heliocentric distances where the constant distance approximation is generally closer to being true over the orbital arc being fit. It is thus an attractive method to try to link Planet Nine over multiple oppositions.

In our implementation, we assume a range for heliocentric distance, $r$ (following Holman et al. 2018, we explicitly assume uniform spacing in $\gamma = 1/r$ from zero to $1/r_{\rm min}$, the minimum distance considered, here set to 200 au), and then, for each detected transient and assumed distance, we calculate the great circle direction and speed required to link every other single transient in the catalog (in practice, we calculate $\dot{\alpha}$ and $\dot{\beta}$, the speed in heliocentric longitude and in latitude). Real objects will appear as a cluster within a fixed range of $\Delta\dot{\alpha}$ and $\Delta\dot{\beta}$ when the assumed distance is close to their correct distance, demonstrating that they are consistent with great circle motion at a constant speed (Figure 3). Depending on our assumed tolerances, sometimes random collections of false-positive transients will also appear sufficiently clustered. To further filter out such false linkages, we take each potential cluster, perform an iterative calculation for the best-fit value of $r$ using the heliocentric Holman approximation, and calculate RMS astrometric residuals, RMS $_{\rm holman}$. All clusters which pass this RMS threshold are passed to a full orbit integrator using the Bernstein geocentric algorithm and a final astrometric residual RMS $_{\rm bernstein}$ threshold is imposed. In regions of high space density of transients, the number of transients, $m$ within a $\Delta\dot{\alpha}$, $\Delta\dot{\beta}$ cluster threshold may exceed the number, $n$, required for a detection. In these cases we create and individually test all ${}_mC_n$ combinations containing $n$ transients independently.

In this method, the five critical parameters to be chosen, each of which affect algorithmic efficiency, are $n$, the number of detections required, the grid spacing of assumed heliocentric distances used, $\Delta\gamma$, the tolerances in heliocentric speed in longitude and latitude, $\Delta\dot{\alpha}$ and $\Delta\dot{\beta}$, and the two RMS astrometric residual thresholds, RMS $_{\rm holman}$ and RMS $_{\rm bernstein}$. The initial step of heliocentric projection and speed calculation involves computationally efficient matrix operations. Each potential cluster that needs to be passed to the iterative calculation for best-fit $r$, however, requires significantly longer computational time, so we attempt to limit the number of these calculations. Fewer false clusters will be found if $n$, the number of required detections, is larger, but then the probability of finding real objects decreases. Smaller numbers of false clusters can also be found if $\Delta\dot{\alpha}$ and $\Delta\dot{\beta}$ are made tighter; however, to do so requires an increasingly finer grid in assumed distances, $\Delta\gamma$, as even real clusters appear dispersed when projected to a sufficiently wrong heliocentric distance. The cluster dispersion problem becomes more acute for objects at smaller heliocentric distances and for observations over larger time spans, both of which begin to stress the assumptions of the Holman et al. (2018) method.

We determine efficient values of these parameters by considering the simulated observations of the Planet Nine reference population. First, for computational efficiency and ease of parallelization, we divide the sky into three-by-three-degree bricks to be processed separately (each brick overlaps adjacent bricks sufficiently that all detections of the fastest-moving object expected will appear within at least one single brick, as verified by our reference population). For each brick, we collect all simulated reference population detections and test our linking algorithm multiple times using a logarithmically-spaced choice for $\Delta\gamma$ and, for each, calculating the minimum values of $\Delta\dot{\alpha}$ and $\Delta\dot{\beta}$ required to link all observations. We then calculate the astrometric residuals after an iterative heliocentric best fit to $r$ and save the maximum value obtained in each brick as RMS $_{\rm holman}$. We also solve each object using the full geocentric integration and likewise save the maximum astrometric residual as RMS $_{\rm bernstein}$. We add $1''$ to each of these RMS parameters to account for the astrometric uncertainties of the real observations. As a computational convenience, for each brick we also calculate upper and lower limits to the speed and direction for all members of the Planet Nine reference population. In our final analysis we will restrict ourselves to only searching for links that are within these limits. At this stage we have appropriate $\Delta\dot{\alpha}$ and $\Delta\dot{\beta}$ for a wide selection of potential choices of $\Delta\gamma$. The final choice of $\Delta\gamma$ and required numbers of detections comes from choosing the

sparsest grid possible and minimum number of detections that do not cause too many initial linkages that need to be checked with the iterative algorithms. In practice we make this choice by examining our most densely populated brick and running a few test cases. For this analysis we find that requiring seven detections and a grid spacing of $\Delta\gamma = 0.0001$ au$^{-1}$ leads to efficient processing. With this choice for $\Delta\gamma$, typical values for $\Delta\dot{\alpha}$ and $\Delta\dot{\beta}$ are $5 \times 10^{-5}$ and $2 \times 10^{-5}$ deg day$^{-1}$, respectively, with clear dependence on ecliptic latitude. Values for RMS $_{\rm holman}$ range from 2″ to 12″ (again, with the major dependence on ecliptic latitude), and a global value for RMS $_{\rm bernstein} = 1$ arcsec is found to be appropriate, which we increase to RMS $_{\rm bernstein} = 2$ arcsec to account for astrometric uncertainties not present in the synthetic reference population data.

An example of the workings of the algorithm can be seen in Figures 2 and 3. One of the members of the Planet Nine reference population, with V = 19.9 and at a current distance of 264.8 au, is predicted to have been detectable 50 times in the ZTF survey. Seen from the Earth, these detections make three loops over the three year survey period (Figure 2(a)). Efficiently linking these observations within a background of randomly placed false-positive detections is a difficult problem. When transformed to heliocentric coordinates at the correct distance (black point in Figure 2(b)), the object travels in a straight line at a constant speed. With our choice of $\Delta\gamma = 0.0001$ au$^{-1}$, the closest assumed distance to the true distance is 263.2 au (with the next closest 270.3 au). Using those values as our assumed distances (red and green, respectively), divergences from the straight line motion begin to appear. Figure 3 shows the speed in heliocentric longitude and latitude required for an object to move from the first position of the orbit to each of the 49 other positions of the orbit. If the correct distance is assumed, these speeds are all nearly identical (black points), demonstrating constant circular motion. At the closest distance in our assumed grid, all of the speeds still fall within the range of $\Delta\dot{\alpha}$ and $\Delta\dot{\beta}$ such that they would be flagged as a cluster to further study. In this particular case, the iterative Holman fit finds a distance of 264.8 au and an RMS of 0.″10. The full Bernstein integration finds an RMS of 0.″30. All 50 detections of this object would be successfully linked across three oppositions.

After selection of algorithm parameters, each brick is ready to be searched for Planet Nine. Before proceeding, we inject the entire data set of simulated observations of the Planet Nine reference population, adding normally distributed errors of 1″ to each astrometric position to conservatively account for the measurement uncertainties in ZTF. While these objects should all be detected by design, embedding them within the real data allows an end-to-end calibration of our search method. Each of the 1164 bricks is processed independently. Of the 56,373 members of the Planet Nine reference population that had seven or more detections that we injected into the data, 56,173, or 99.66% were detected and linked. Our algorithm is extremely efficient at successfully linking detections over the full three year period for these distant objects.

In the full ZTF data set, 103 potential linkages made it to the final step of full orbital integration using the Bernstein integration method—including one with as many as 23 linkages—and all but one failed this final cut. The single object that survived the final cut was, surprisingly, Eris. Eris is coincidentally along the predicted P9 path, but the search algorithm was not optimized to find objects at a distance of only 96 au. Nonetheless, Eris was successfully linked owing to a string of 11 detections in 20 days that occurred close to quadrature when the motion of Eris could not be distinguished from that of a more distant object. We examined each of the 102 other linkages individually and did not find any reason to consider them further. Planet Nine was not detected in the ZTF data.

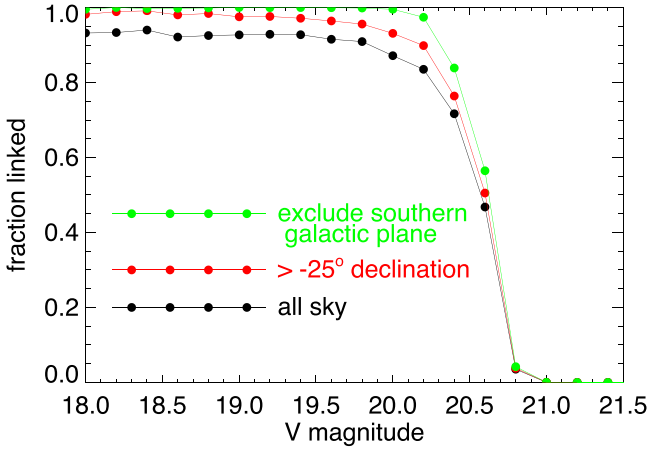


**Figure 4.** Limits to the detection of the Planet Nine reference population in the ZTF data. Across the entire sky 91% of the brightest objects are detected. If we exclude areas south of −25° decl., 94% are detected, and if we exclude the poorly observed southern hemisphere galactic plane region, 100% of the bright objects are detected.

## 6. Planet Nine Detection Limits

With no detection of Planet Nine in the data set we use the Planet Nine reference population to determine limits across the search region. Our simplest metric is the fraction of the 100,000 members of the Planet Nine reference population that would have been detected. Our algorithm would have found 56,173 members of the reference population in ZTF across the full sky. The brightest members of the population are most efficiently detected, as shown in Figure 4. The ZTF survey would have successfully identified ∼92.4% of all members of the Planet Nine reference population with $V < 19.75$, with a 50% efficiency at $V = 20.57$. Many of the bright objects that were not linked were further south than the decl. limit of the ZTF survey. If we examine the fraction of objects successfully linked that have declinations above −25°, we find the the survey linked 95% of the bright objects, with a 50% efficiency at $V = 20.60$. Of the bright objects within the ZTF survey region, the other source of missed detections is the poorer coverage in the southern galactic plane. If we exclude the southern regions with galactic latitude less than 15° we detect 99% of the objects brighter than $V = 20.0$ and a 50% efficiency at $V = 20.62$.

To better examine the spatial structure of the detection limits, we again use our synthetic population, and we determine the brightest synthetic Planet Nine that is missed at each HEALPix. We define the limit as the next-brightest object from this first missed object. A map of these limits is show in Figure 5, which also conveniently shows the Planet Nine search region. For the Planet Nine search region, the limits found from the Planet Nine reference population are nearly identical to those of Figure 1 determined for asteroids. The asteroid limits, requiring

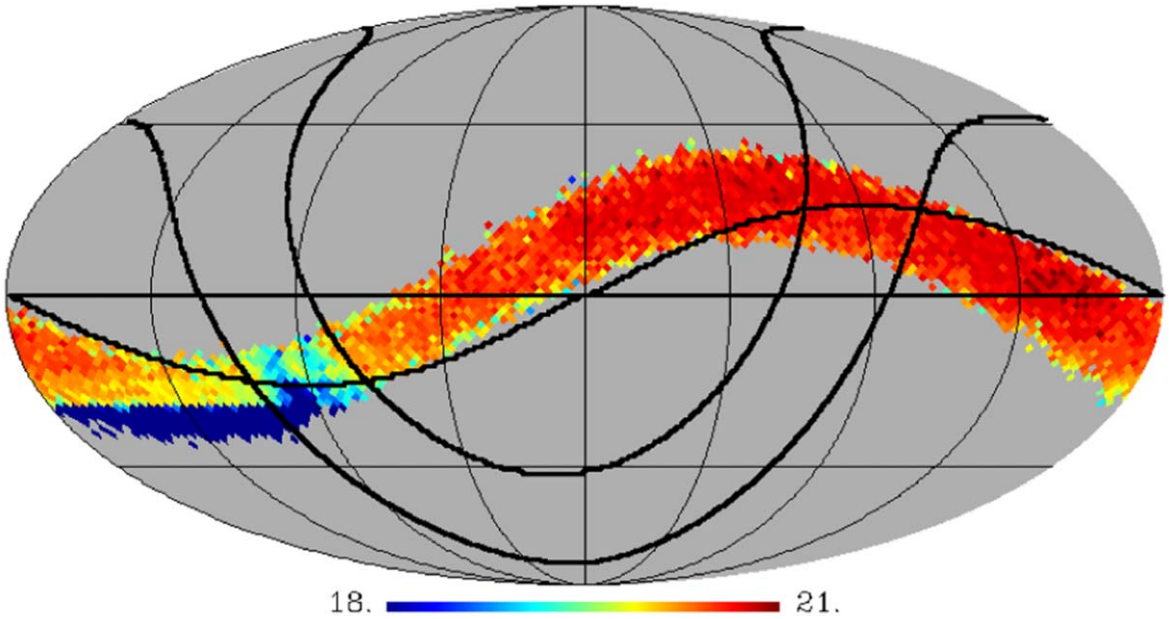


**Figure 5.** Detection limits across the Planet Nine search region determined from the search for objects from the Planet Nine reference population injected into the data stream. The geometry of the project is identical to that of Figure 1. The dark blue regions in the southern hemisphere are areas not covered by ZTF.

a 95% detection efficiency, are better sampled and better defined than the synthetic Planet Nine limits, so we regard the asteroid limits of Figure 1 the magnitude limits of the full survey.

## 7. Discussion

The results presented here provide a useful framework for understanding our current limits on the detection of Planet Nine and for incorporating additional surveys into the limits. Any survey can use the the full reference population of 100,000 synthetic Planets Nine to inject samples from the BB21 analysis and determine if they are detected. Each reference object contains full orbital elements as well as mass, assumed radius, and assumed albedo, and can be used to calculate positions, distances, magnitudes, thermal fluxes, and gravitational forces at any survey time. Different assumptions about radius and albedo can easily be incorporated into the population. The full reference population[5] also indicates which objects from this population would have been detected in the ZTF survey. The table of potential detections will be expanded as additional surveys use this reference population and determine which objects they should have detected.[6] The reference population as well as the list of objects which should have been detected can easily be used to recreate Figures 4 and 5 for the current survey and equivalent visualizations for all surveys that are included.

The website also hosts full HEALPix limit map equivalent to Figure 5 and will provide updates for any additional surveys which publish equivalent limits. This map will be able to be used to quickly discern which areas of the sky have had published surveys contributing to the global limits on Planet Nine, with the important caveat that the limits presented here, at least, are only for objects with roughly the orbital characteristics predicted for Planet Nine by BB21.

[5] Hosted at https://data.caltech.edu/records/2098 (Brown 2021).

[6] Contact the first author to include analysis from a survey into the reference population tables.

These are the first rigorous optical limits placed on the existence of Planet Nine over nearly the full predicted search area. This survey could have detected more than 56% of the P9 reference population. Given the assumptions of radius and albedo that we used for the reference population, we can update expected Planet Nine parameters. The remaining population has 15.9, 50.0, and 84.1 percentile values for mass of $6.3^{+2.3}_{-1.5}$ Earth masses, semimajor axis of $460^{+160}_{-100}$ au, perihelion of $340^{+80}_{-70}$ au and aphelion of $560^{+260}_{-140}$ au. The other parameters are generally unchanged. Not surprisingly, a survey ruling out more than half of the most bright parameter space pushes the expected orbit of P9 further away.

The method that we have developed here for both detection and calibration of transient surveys is applicable to many other existing surveys. Given the potential of a brighter Planet Nine than original anticipated, such searches could prove fruitful.

This research has benefited greatly from conversations with Rich Dekany, Matt Holman, Matt Payne, and Matthew Belyakov. An anonymous referee provided insightful comments that improved the presentation of this manuscript.

## ORCID iDs

Michael E. Brown https://orcid.org/0000-0002-8255-0545
Konstantin Batygin https://orcid.org/0000-0002-7094-7908

## References

Batygin, K., & Brown, M. E. 2016, AJ, 151, 22
Bellm, E. C., Kulkarni, S. R., Graham, M. J., et al. 2019, PASP, 131, 018002
Bernstein, G., & Khushalani, B. 2000, AJ, 120, 3323
Brown, M. 2021, Planet Nine reference population, v1.0, doi:10.22002/D1.2098
Brown, M. E., Bannister, M. T., Schmidt, B. P., et al. 2015, AJ, 149, 69
Brown, M. E., & Batygin, K. 2021, AJ, 162, 219
Fortney, J. J., Marley, M. S., Laughlin, G., et al. 2016, ApJL, 824, L25
Holman, M. J., Payne, M. J., Blankley, P., Janssen, R., & Kuindersma, S. 2018, AJ, 156, 135
Masci, F. J., Laher, R. R., Rusholme, B., et al. 2019, PASP, 131, 018003
Wu, Y., & Lithwick, Y. 2013, ApJ, 772, 74